© Copyright by Yongtian He 2018
All Rights Reserved

NEURAL DECODING OF WALKING IN STROKE

A Dissertation

Presented to

the Faculty of the Department of Electrical and Computer Engineering

University of Houston

in Partial Fulfillment

of the Requirements for the Degree

Doctor of Philosophy

in Electrical Engineering

by

Yongtian He

December 2018

NEURAL DECODING OF WALKING IN STROKE

Yongtian He

Approved:

Chair of the Committee
Jose L. Contreras-Vidal, Professor
Department of Electrical and Computer Engineering

Committee Members:

Saurabh Prasad, Assistant Professor
Department of Electrical and Computer Engineering

Rose T. Faghih, Assistant Professor
Department of Electrical and Computer Engineering

Yingchun Zhang, Associate Professor
Department of Biomedical Engineering

Gerard E. Francisco, M.D., FAAPMR, Chair
Dept. Physical Medicine and Rehab., UT Health
Chief Medical Officer, TIRR Memorial Hermann

Suresh K. Khator, Associate Dean
Cullen College of Engineering

Badrinath Roysam, Chair
Department of Electrical and Computer Engineering

Acknowledgements

This dissertation is dedicated to my parents Zeng Huaping and He Dongyi. Bitter or sweet, they walked with me in every step in my life.

I also want to thank those whose direct or indirect contribution made this dissertation possible.

My PhD advisor Dr. Jose (Pepe) Contreras-Vidal gave me tremendous support throughout my graduate program. I benefited greatly from his rigorous training. More importantly, he showed me soft skills such as independent problem solving and professional communication. For that he will have my gratitude forever.

I appreciate Dr. Prasad, Dr. Faghih, Dr. Zhang, and Dr. Francisco for serving on my dissertation committee and giving me professional advice. Dr. Layne and Dr. Gorniak from the UH CNBR generously provided space and equipment in the Texas Medical Center in my early projects. Dr. Trieu Phat Luu's mentorship and friendship helped me significantly during these years.

I'd like to thank my subjects with stroke who voluntarily came day after day for the experiments. Some of you had to take the MetroLift which took forever to show up. When my work seemed to hit walls, your encouragement to carry on meant a lot to me. You are the true hero behind my research.

I also want to thank my amazing colleagues in the UH BMI lab, the most diverse place I've ever experienced. Luu, Sho Nakagome, Alex Craik and Kevin Nathan assisted me during the data collection. Luu, Sho, and Samual Brown contributed significantly in the software development. Andrew Paek, my roommate and my first new friend in the U.S., is probably the warmest person I've ever met. His corny jokes cracked my culture and language barriers like magic. Justin Brantley will be the first person I text when I

can bench press 135 lbs. I sincerely enjoyed the company from every single student in the lab.

My special thanks go to my long time friends Qin Kun and Zhang Yu, who are always there to encourage me whichever timezones life brings us to.

NEURAL DECODING OF WALKING IN STROKE

An Abstract

of a

Dissertation

Presented to

the Faculty of the Department of Electrical and Computer Engineering

University of Houston

in Partial Fulfillment

of the Requirements for the Degree

Doctor of Philosophy

in Electrical Engineering

by

Yongtian He

December 2018

Abstract

Stroke is a leading cause of long-term disability in the U.S. and does not have an effective cure yet. Most post-stroke motor rehabilitation programs rely on physical therapy, which focuses on manipulating affected limbs. However, such programs only indirectly engage the cause of the symptoms: the damaged brain areas. Brain-computer interfaces (BCI) are systems that use brain activity to control external devices, allowing direct monitoring and involvement of patients' brains. To explore this novel stroke rehabilitation paradigm, three subjects with chronic stroke were recruited. They walked on a treadmill while controlling a virtual humanoid avatar on a TV through their brain signals. This real-time control was implemented based on a Kalman filter which predicted the subject's joint angles using their electroencephalogram (EEG) in the delta band (0.1–3 Hz). The performance was measured by Pearson's correlation coefficient r between the actual and predicted joint angles. This closed-loop BCI training paradigm was repeated for 16 trials during 8 days for each subject. Results show that promising performance was achieved ($r = 0.60, 0.59, 0.30$ for the three subjects). Significant cortical adaptation was found in the delta and theta band EEG across trials. The delta band EEG, which drove the BCI decoder, was significantly associated with the decoder performance. Various motor learning effects were observed, including improved spatial and temporal gait consistency, and bilateral symmetry. The present study is the first BCI protocol designed for stroke rehabilitation in the context of walking. The promising BCI performance was backed up by significant correlations in EEG brain features, and more importantly, by the subjects' motor function improvement. The reported training paradigm may elicit several key adaptations in the EEG and motor skills of the chronic stroke survivors, which could lead to a new generation of stroke rehabilitation programs.

Table of Contents

Acknowledgements **v**

Abstract **viii**

Table of Contents **ix**

List of Figures **xi**

List of Tables **xii**

1 Introduction **1**

1.1 Stroke Rehabilitation 1

1.2 Brain-computer Interfaces 2

1.3 Walking 3

1.4 Specific Aims 4

1.5 Innovations 6

2 Methods **8**

2.1 Participants 8

2.2 Data Collection 8

2.3 Protocols 11

2.4 Preprocessing 14

2.5 Decoder 14

2.6 Offline Preprocessing 20

3 Neural Decoding **22**

3.1 Metrics 22

3.2 Results 22

3.3 Discussion 25

4 Cortical Plasticity **28**

4.1 Metrics 28

4.2 Results 28

4.3 Discussion 30

5 Motor Adaptation **32**

5.1 Metrics 32

5.2 Results 34

5.3 Discussion 37

6 Conclusion **38**

6.1 Future Directions 38

6.2 Summary 40

References **41**

List of Figures

2.1 EEG Montage 10

2.2 Goniometer Setup 12

2.3 Experiment Protocols 13

3.1 Gait Segmentation 23

3.2 Decoder Performance in Each Gait Cycle 24

3.3 Histogram of Decoder Performance 25

3.4 Decoder Performance over Days 26

4.1 Correlation between EEG and Performance 29

4.2 Train-test Difference in Delta EEG 30

4.3 Theta EEG Power Increase 30

5.1 Gait Trajectory Centroid 33

5.2 Temporal Gait Consistency 35

5.3 Spatial Gait Consistency 36

5.4 Bilateral Symmetry 36

List of Tables

2.1 Participant Eligibility Criteria 9

2.2 Subject Demographics 9

Chapter 1

Introduction

1.1 Stroke Rehabilitation

Stroke is a leading cause of long-term disability in the U.S. and does not have an effective cure yet. It usually affects one's contralateral motor control ability [1]. Chronic stroke survivors, who are often seen walking with over-compensating postures [2], need to re-learn correct gait patterns in their rehabilitation. How to effectively enable the recovery of damaged neural mechanisms in the brain remains an open question with great significance. Current recommended treatments for gait rehabilitation are based on repetitive physical training [3], which usually requires significant physical labor from physical therapists as they manually lift and move patients' legs as they walk in rehabilitation facilities. Recently, robot-assisted therapies are gaining popularity as they provide repetitive and long-duration training.

However, there are several limitations with these approaches. First of all, therapists lack direct tools to interact with patients' brains. Stroke is by definition a trauma to the brain. Yet most motor rehabilitation therapies primarily interact with the patients through their extremities. The reason might be that human brains have historically been and currently still less understood than the motor functions in limbs. For the most part in human's medicine practice history, we lacked ways to directly interact with the brains. Although modern neural imaging technology could pinpoint the site of the stroke in brain, how the brain adapts and recovers after stroke is not well understood.

Secondly, it is difficult to monitor the recovery progress of stroke. Clinical improvements of the patients are usually measured by high-level metrics such as Fugl-Meyer score,

10-meter walk test, etc. While they are by all means necessary, they only monitor the functional outcome instead of the source of stroke: the brain. Besides, due to their nature, it is impractical to monitor these metrics in real-time during therapies.

Thirdly, it is challenging to retain the active engagement of the patients during assisted motor tasks. As cognitive deficits affect both patients' memory and attention, the provision of continuous instructions both physically and verbally may be overwhelming and therefore less effective [4]. Active contribution to physical movements is critical for the encoding of motor memory [5, 6]. The voluntary engagement in exercise has been proved be relevant in various stroke rehabilitation protocols, such as spatial neglect disorder [7], robotic gait training [8, 9], upper extremity exercise robotics [10] and music therapy [11].

1.2 Brain-computer Interfaces

With the recent understanding and development of brain-computer interface (BCI), it has been proposed as a novel tool in motor rehabilitation [12]. BCIs are systems allowing brains to directly control external objects, which can be either hardware or software. The feasibility of using BCIs to control robotics was first demonstrated with invasive BCIs in upper limb applications with both non-human primates [13, 14] and humans with tetraplegia [15, 16, 17]. However, these approaches face the risk of surgical complications and infections, short-term and long-term signal instabilities that degrade neural decoding of intent [18], and the challenge of maintaining stable chronic recordings [19]. The added risks associated with the testing of BCI systems for lower-limb applications preclude the development of invasive BCIs for lower limb applications in humans [20].

In order to mitigate or eliminate safety risks and reach a broader clinical population, the scalp electroencephalogram (EEG) has been used as a non-invasive alternative for BCI applications. Progress has been made in controlling virtual objects [19, 21], upper

limb robotic devices [22, 23], and wheelchairs [24, 25, 26]. Specifically, EEG has also been recently used to monitor cortical activity during walking-related tasks because of its portability and high temporal resolution [27, 28, 29, 30, 31].

EEG has previously been studied in the context of rehabilitation prediction after stroke. A review of 15 studies concluded that delta/alpha power ratio and broadband voltage asymmetry between hemispheres are statistically significant predictors of outcomes assessed (via routine clinical scales) [32]. It was reported in [33] that pre-movement EEG can predict the intention to walk in stroke patients. However, there are not enough clinically proved evidence to use EEG as an indicator clinically in stroke.

1.3 Walking

Most of current EEG-based BCI studies examined EEG when users performed upper limb functions, such as reaching and grasping [16, 23]. Compared to upper-limb, protocols involving lower-limb motor functions introduce two extra burdens: logistics and EEG artifacts.

1) Logistics: In most upper-limb protocols the subjects remain seated, so that the subjects, experimenters, and equipment can all stay still. The benefits are obvious: 1) it is certainly easier to manage; 2) it allows wired connections between equipment, which suffers less from the loss and lag during data transmission. For lower-limb protocols, part of this burden can be mitigated by walking on a treadmill instead of overground.

2) EEG artifacts: Scalp EEG inherently contains various types of artifacts, a lot of which may be amplified during motion. For instance, muscles on the neck may involuntarily tighten to keep balance during walking, resulting in larger electromyography (EMG); motions may cause cables on the EEG cap to rub against each other, affecting the electrical field; prolonged walking leads to sweating on the head, changing electrical property of the scalp over time. Artifact removal during walking has only been explored in the re-

cent decade. Artifacts produced by gel displacement during walking have been carefully characterized [34]. Computational models were validated to remove movement-related artifacts in EEG during walking [35, 36, 37, 38]. Lately, several groups have extensively studied motion artifacts in EEG. A delicate insulated head model was developed to characterize signal-to-noise ratio during lab-controlled motions [39]. Results showed that the artifacts can be significantly reduced using independent component analysis (ICA). Interestingly, motion artifacts were found to be negligible with careful experimental setup and when low speed is maintained [40]. This insight creates opportunities to use delta band EEG in gait rehabilitation where the walking speed is usually slow.

Evidence suggests that EEG recordings during walking display distinct features that differ from those observed during standing, and more importantly, are coupled with gait cycles [28, 29, 30, 41, 42]. However, a real-time interface between the affected brain regions and the patient/physician has yet to be established in the context of gait rehabilitation.

1.4 Specific Aims

To fill the gap between EEG and stroke rehabilitation, I have been leading the project of designing a real-time BCI for gait rehabilitation after stroke. The BCI serves as a novel tool for the patients to have neural engagement during the task, and for physicians and therapists to better monitor their progress. EEG from the chronic stroke patients were recorded non-invasively during treadmill walking. Meanwhile, a real-time decoder was trained to predict the lower limb movement of the subjects. This prediction was visualized by projecting it to a virtual avatar on a screen, thus forming closed-loop brain control. This BCI system had been tested offline [43], and also validated online with healthy subjects [44]. To my best knowledge, the present study is the first closed-loop BCI for gait rehabilitation in the stroke population.

This dissertation consists of three specific aims, with their results detailed in Chapters 3 through 5:

Aim 1 (Neural Decoder): To develop an EEG-based non-invasive BCI for chronic stroke patients to control a virtual avatar for gait rehabilitation. Unscented Kalman Filter was used to model the non-linear correlation between the EEG and the joint angles. The performance of the decoder was measured by the correlation coefficient between the measured and predicted joint angles on the lower limbs of the subjects. High accuracy would suggest that the EEG-based BCI is promising to the stroke population as an assistive and rehabilitative tool.

Aim 2 (Cortical Plasticity): To study the short-term and long-term adaptive responses in EEG brain waves triggered by the BCI. EEG features in certain bands are known to couple with gait cycles [41] and different types of walking tasks in healthy subjects [45]. The findings from this study with the clinical population have important implications in monitoring and improving the post-stroke rehabilitation using EEG.

Aim 3 (Motor Adaptation): To examine the adaptations in the kinematics and the level of control by the subjects. With the multi-day training protocol design, subjects became experienced and learned from the BCI-avatar task progressively. The change in their motor control and confidence level was quantified over time. These metrics provide insights on the progress of the kinematics gait adaptation to the BCI tasks in stroke survivors.

Gait rehabilitation is an essential part in improving the quality of life of the patients with chronic stroke. The presented closed-loop BCI allows patients to directly engage their brain during training, while also provide a non-invasive interface for the physicians to quantitatively monitor brain activities and kinematics. This information is valuable to advance our knowledge about changes in EEG and BCI performance in the stroke population in the context of rehabilitation of walking, which has not been previously

reported.

1.5 Innovations

Prior work of EEG-based BCIs related to lower limb applications roughly fall into three categories: active orthoses [46], exoskeletons that assist walking [20], and virtual avatars [47, 48]. Regardless of the type of end effectors, previous BCI studies usually lack one or more of the following principles to address the stroke population.

Firstly, rehabilitation-focused study designs are lacking. While there were plenty of research about arm prosthetics [49] and finger tapping [50], few studied gait rehabilitation. There are only a few studies reporting discrete classifications of high level walk-related commands, such as moving, stopping, and turning [47, 48, 51, 52]. While they guide assistive devices for ambulation, they do not generate cortical activities that are directly relevant to performing gait cycles. For example, users were instructed to focus on different visual stimuli in a study based on steady-state visual evoked potentials (SSVEP) [52]. In another exoskeleton-based study, users were instructed to imagine a specific arm or leg contraction in order to initiate the device to carry out an entire gait cycle [53]. Additionally, many studies were conducted on a single day for each subject and long term effects may be overlooked. The present study enables BCI users to use their brain to control a virtual avatar on screen to walk by controlling its joint angles. The direct joint control is directly relevant to the gait rehabilitation in stroke.

Secondly, many related studies were evaluated offline [51, 54, 55], which may not be readily available in real-time. Some commonly used offline techniques, such as Independent Component Analysis (ICA), Principle Component Analysis (PCA), spectral analysis, and outlier rejection are not available in real-time scenarios. In the present study, consideration has been put in each step to enable real-time. Denoising and decoding were implemented with customized C++ programs in real-time. A digital avatar

was developed with Unity engine to provide real-time visual feedback in a virtual environment.

Thirdly, the participant population in many studies were solely healthy subjects, as in [44, 52, 56]. The characteristics of EEG in stroke is still a largely unanswered topic [57], and it is not uncommon to see results vary across groups in EEG studies that enrolled both the healthy and stroke population [51, 58]. Studies that were designed for the stroke may yield more relevant results if they incorporate this population into their cohort.

Chapter 2

Methods

2.1 Participants

People with chronic stroke (more than 6 months since their last stroke attack) were invited to participated in this study. Medical screening was performed to ensure subjects have enough ability to walk on a treadmill safely and independently. The eligibility criteria are listed in Table 2.1. Three qualified subjects were enrolled. Written consent was acquired from each subject. This experiment was approved by the Institutional Review Board (IRB) at the University of Houston.

The three subjects are all male, average age 38.3 $\pm$ 8.5 years old. Coincidentally, they all have stroke in the right hemisphere, resulting in varied degrees of paralysis on the left side of the body. Table 2.2 shows the demographic and clinical information of the participants. Throughout the rest of this dissertation, they are usually referred to by their de-identified ID: *S1*, *S2*, and *S3*.

All three subjects scored 30 in Mini mental state exam, suggesting their mental abilities are not reduced at the time of the experiment. Their physical conditions all fit the criteria: they have some levels of paralysis, but are still able to walk independently.

2.2 Data Collection

Whole scalp 60-channel active EEG and 4-channel EOG activity were collected (ActiCap system, Brain Products GmbH, Germany) and labeled in accordance with the extended 10-20 international system (Figure 2.1). A RF wireless interface (MOVE system, Brain Products GmbH, Germany) was used to transmit data to the host PC

Table 2.1: Participant eligibility criteria.

Inclusion Criteria

- Presence of unilateral hemiplegia
- Chronic stroke i.e., interval of at least 6 months from stroke to time of enrollment, respectively;
- Aged between 18-60;
- Have no contraindications to standing or walking; able to stand with assistive device for at least 5 minutes;
- Cognitive ability to consent, assimilate, and participate actively in the treatment protocol (Mini Mental State Examination score > 24 points, out of a total 30 indicating normal cognitive ability);
- Modified Rankin scale scores 1-3 (Mild-Moderate functional disability post-stroke);
- Modified Ashworth Scale of Spasticity score <= 2 (ranges from 0-4 with 4 reflecting maximum spasticity);

Exclusion Criteria

Individuals with stroke who have been diagnosed with cognitive or severe visual deficits, neurological conditions other than stroke, hemineglect, uncontrolled angina, or pregnancy

Table 2.2: Demographic and clinical information of the subjects. Acronyms: R: Right; MCA: middle cerebral artery.

Subject ID	*S1*	*S2*	*S3*
Age (year)	32	35	48
Gender	M	M	M
Height (cm)	182	185	195
Weight (kg)	86	111	98
Hemiparesis	Left	Left	Left
Stroke	R Basal ganglia	R Frontal lobe	R MCA
Onset (month)	156	11	53
Fugl-Meyer LE (0-34)	31	28	17
Modified Rankin Scale (0-5)	2	3	2
Mini Mental State Exam (0-30)	30	30	30

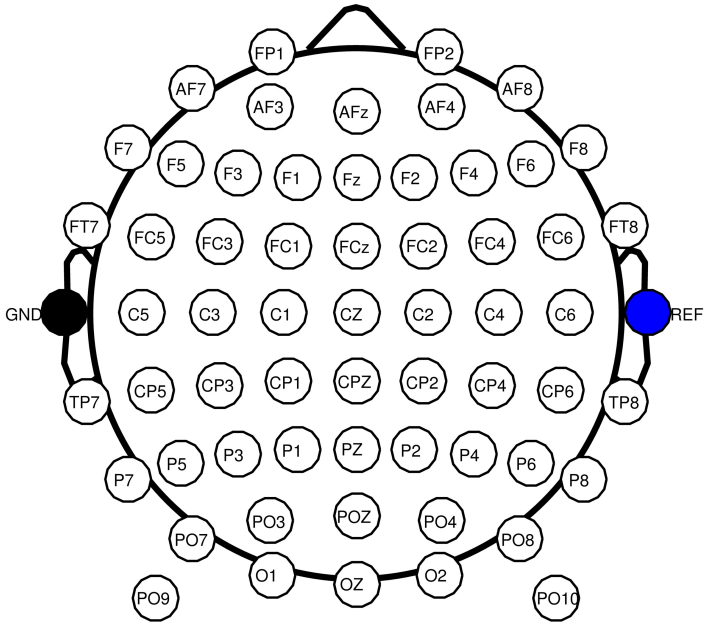

Figure 2.1: Customized EEG channel montage. Ground (GND) and Reference (REF) are located on the left and right earlobe.

at its default working band. The data were recorded at 100 Hz. Ground and reference channels were placed on the left and right earlobe respectively (A1 and A2). Channels T7 and T8 were subsequently moved to FCz and AFz, where the ground and reference channels were originally positioned. This change allowed better sensor coverage of the parietal and frontal areas of the cortex. Sensors at FT9, FT10, TP9, and TP10 were moved to locations around the eyes (lateral sides of the eyes by the temples, and superior and inferior to the left eye) to capture ocular activities (electrooculogram, EOG): TP9, above the left eye; TP10, below the left eye; FT9, left of the left eye; and FT10, right of the right eye. Conductive gel (SuperVisc, Brain Products GmbH, Germany) was applied between sensors and the scalp to maintain impedances below 60 kΩ. Channel impedance were recorded after each gelling process.

Bilateral joint angles on the legs (hip, knee, and ankle) in the sagittal plane were

recorded by six goniometers (Biometrics Ltd, UK) at 100 Hz. Subjects wore compression shorts for easier placement of the goniometers on the hips to reduce interference from clothing. We first attached all six goniometer sensors to customized 3D printed applicators, then donned them to the subject with double-sided medical tape. The custom applicators maintain a neutral length in the goniometer springs and ensure repeatability. This procedure is illustrated in Figure 2.2.

The EEG and goniometer data were synchronized in real-time using a designated PC application. The software was developed mainly in a C++ framework. The IT++ library (http://itpp.sourceforge.net/4.3.1/index.html) was used for mathematical computation . The output of the decoder was sent to a Unity game engine (https://unity3d.com/) to drive the animation of a virtual avatar.

2.3 Protocols

Assessments (Lower-extremity Fugl-Meyer Score, Modified Rankin scale, and Mini Mental State Examination) were administered before the first trial in order to examine the subjects eligibility. The subjects were invited to participate in a total of 16 identical BCI trials that were scheduled on eight different days, two on each day. They were encouraged to take sufficient rest between the two trials on each day. These eight days of appointments were scheduled as close as possible, with a total span of less than a month for each subject. S1 finished all 16 trials. S2 missed the second trial on his second and fourth day because of schedule conflicts. Similarly, S3 missed the second trial on his first, second, and fourth day. To sum up, S1, S2, and S3 completed 16, 14, and 13 trials respectively.

At the beginning of each trial, the subject was asked to stand still for 30 seconds to serve as a baseline period, followed by 20 minutes of continuous walking on a treadmill (Figure 3). The treadmill speed was controlled by the experimenter and kept at a low

Figure 2.2: Illustration of the goniometer setup procedures. a) Attach goniometers onto the joint. b) Measure the distance to ground as a guidance for the goniometer placement on the other leg. c) Final position of hip, knee, and ankle goniometer units.

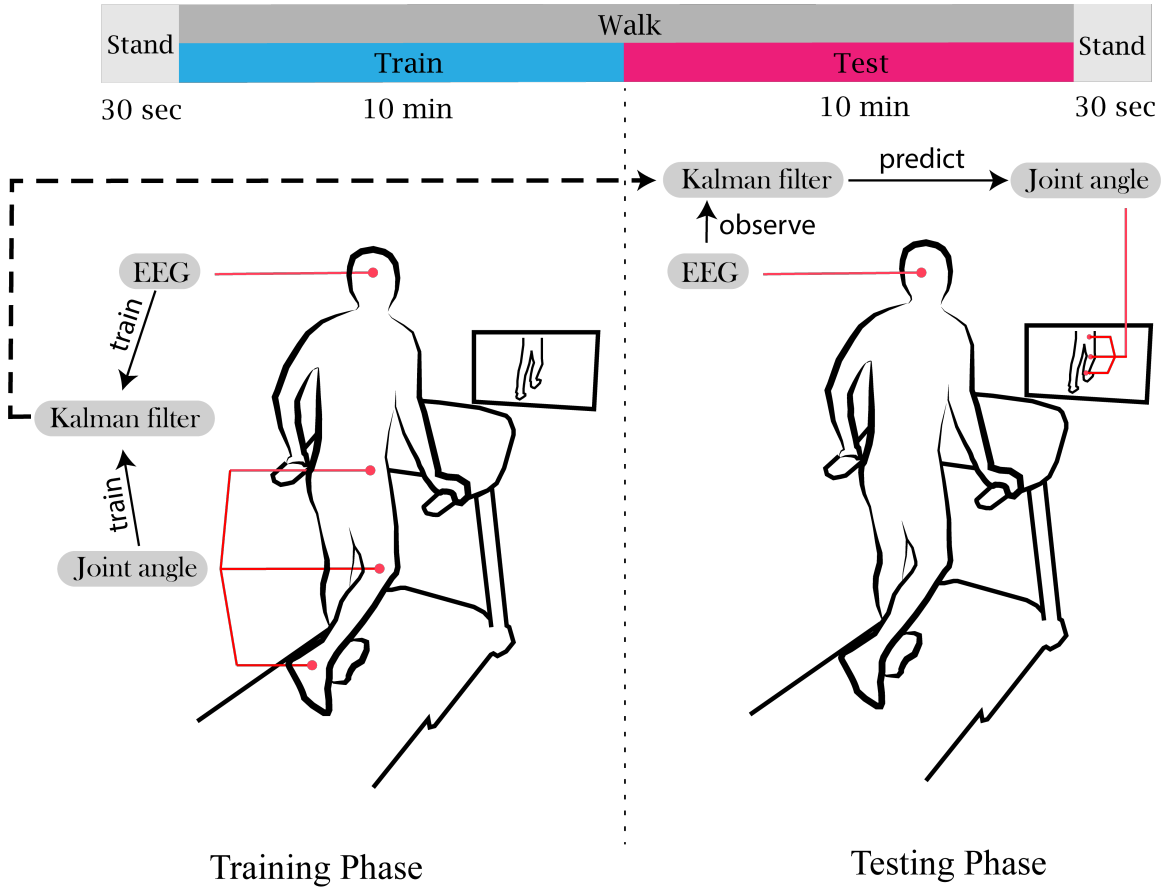

Figure 2.3: Illustration of the experiment protocols. Each trial contains two 10-min periods of walking: training and testing phase. In both cases, the subject walked on a treadmill while the virtual avatar in TV followed his movement.

speed (1 mile per hour, roughly 0.45 meter per second).

A screen was placed in front of the treadmill for the subject to visualize an avatar of him/herself walking in a hallway. Only the lower body of the avatar was shown on screen (Figure 2.3).

In the first 10 minutes of the walk, subject's joint angles as measured by goniometers were projected to the avatar on screen. The avatar visually followed the movement of the subject. The neural decoder was trained in this period. Therefore, it was named the *training phase*. Afterwards, the avatar's leg on the affected side was switched to be driven by the subject's brain activity. In all three subjects, the brain-controlled side was their left side. A closed-loop brain-control of the avatar was therefore created for this

phase. This phase was named the *testing phase*.

After the walk, the subject stood still for another 30 seconds and completed the trial. Sufficient rest was allowed and encouraged before the start of the next trial. This procedure was repeated two times every day, except for those days when the subjects had to leave early.

2.4 Preprocessing

The same software used in data collection also handled real-time EEG processing and decoding. The 4-channel EOG (Channel FT9, FT10, TP9, and TP10) were used as input to a real-time H∞ filter to remove ocular artifacts. It is based on an adaptive noise cancelling framework that updates at every sample [59]. During the closed-loop BCI, reference signals (EOG) were used to remove noise in the target signal (EEG). The reference signal r at time t is defined as

$$r_t = [TP9_t - TP10_t, FT9_t - FT10_t]^T, \tag{2.1}$$

which is a two-element vector that describes the vertical and horizontal eye movements.

Peripheral EEG channels were then removed as they are most susceptible to artifacts from head movements, and facial/cranial muscle activity. After the removal, there were 48 out of 60 channels remaining. Note that the removal was only implemented during real-time procedures as better methods were used in offline processing, as described in the later section. A 2nd order real-time Butterworth band-pass filter was used to extract delta band (0.1–3 Hz) EEG.

2.5 Decoder

An unscented Kalman filter (UKF), which is a variation of the Kalman filter, was used to predict joint angles from EEG in real-time. Kalman filter is an algorithm that

recursively uses a series of measurements observed over time, models the signal and noise' statistical model, and tends to make better predictions than those relying on a single measurement. From a theoretical standpoint, Kalman filter is a Bayesian model similar to a hidden Markov model but where the state space of the latent variables is continuous and where all latent and observed variables have a Gaussian distribution. UKF improves upon the classic Kalman filter by using a group of seeded samples (sigma points) to model the above steps nonlinearly. It was shown that UKF outperformed the vanilla Kalman filter and the Wiener filter in both offline and real-time BCI operation [60] .

The rest of this section was developed largely based on the UKF proposed in [60], which includes detailed implementation of UKF in the context of neural decoding. However, some of its mathematical notations are not clearly or consistently defined: 1) Q and R matrices on Page 14–15 are only briefly mentioned as "covariance of the noise", which does not capture their physical origin; 2) the transition matrix was noted as B on Page 16 in the paper, but noted as H throughout its Supplemental Materials. To avoid confusion and improve readability, the Kalman filter and its parameter fitting are formally introduced in the following subsections. Different notation styles were reviewed [61, 62]. The style adopted here is commonly used and also close to [60]. To avoid repeating previous work, please refer to [60] for the detailed implementation of the "unscented" flavor of Kalman filter.

Problem Statement

In general, the Kalman filter model tries to estimate the latent state x of a discrete-time controlled process that is governed by the linear stochastic difference equation

$$x_t = F_t x_{t-1} + w_t \tag{2.2}$$

with a measurement

$$z_t = H_t x_t + v_t, \tag{2.3}$$

where

- x_t is the state vector
- z_t is the vector of measurements
- F_t is the state transition matrix which applies the effect of each system state parameter at time $t-1$ on the system state at time t
- H_t is the transformation matrix that maps x_t into the measurement domain
- w_t is the vector containing the process noise terms in the state vector
- v_t is the vector containing the measurement noise terms

In this specific neural decoding scenario the latent state variable x, which is a vector of joint angles, at time t, was defined as

$$x_t = [\theta_{rh}, \theta_{rk}, \theta_{ra}, \theta_{lh}, \theta_{lh}, \theta_{lh}]^T, \tag{2.4}$$

where θ represents the angle on a specific joint at time t. Subscripts l and r are short for *left* and *right*; h, k, and a are short for *hip*, *knee*, and *ankle*, respectively. Note that although joints on the right (unaffected) leg were not involved in the real-time brain control, they were still predicted for later analysis.

The measurement vector z_t was defined as a vector of 48 channels of EEG recording at time t. The Kalman filter's task was to use z_t to estimate x_t at each time step. In order to make this task more tractable, a few mathematical assumptions were granted:

1. In theory, the noise term w_t and v_t, and the state matrices F_t, B_t, and H_t might change with each time step or measurement. Here they were assumed to be constant, which a common practice in Kalman filter applications [60].

2. The process noise w_t and measurement noise v_t were assumed to be zero mean Gaussian white noise:

$$w \sim N(0, Q) \tag{2.5}$$

and

$$v \sim N(0, R). \tag{2.6}$$

As a result, the governing equation of the Kalman filter Eq. 2.2 and Eq. 2.3 are simplified into

$$x_t = Fx_{t-1} + w \tag{2.7}$$

and

$$z_t = Hx_t + v. \tag{2.8}$$

Parameter Fitting

The metrics F, H, Q and R were fitted using the data recorded during the training phase in each trial. Like the testing phase, the training phase data included both joint angles (state variable x_t) and EEG (measurement z_t) of the subjects. The joint angles were composed into a $d_1 \times T$ matrix X, where $d_1 = 6$ is the number of joints being monitored, and T ($\approx$ 10 minute $\times$ 100 Hz) is the total number of data points. It should be noted that the EEG and joint angle data were augmented with additional time lags in [60], but not in the present setting for faster real-time implementation. A second matrix X_{shift} was then constructed where all columns in X was shifted to the left by 1 step, representing the state variables at one time step later. To avoid the problem of missing data, both X and X_{shift} were kept at $T - 1$ columns when fitting F:

$$FX = X_{shift}. \tag{2.9}$$

To improve the generalization ability of F and to avoid over-fitting, the above

equation was solved using the Tikhonov regularization technique called ridge regression:

$$F = X_{shift}X^T(XX^T + \lambda_F I)^{-1}, \tag{2.10}$$

where I is the $d_1 \times d_1$ identify matrix and $\lambda_F = 4$ is the ridge regression parameter optimized during offline pilot testing.

The movement model noise covariance matrix Q was estimated using

$$Q = \frac{E_F E_F^T}{T - d_1}, \tag{2.11}$$

where E_F is the $d_1 \times (T-1)$ residual matrix from fitting F

$$E_F = X - FX_{shift}. \tag{2.12}$$

Similar to matrix X, the EEG data were composed into a $d_2 \times T$ matrix Y, where $d_2 = 48$ is the number of EEG channels being used in real-time. Columns in X and Y are synchronized. In order to define a more sophisticated neural model H, X was further augmented that each sample $x = [x_{rh}, x_{rk}, x_{ra}, x_{lh}, x_{lk}, x_{la}]$ in X was expanded and re-indexed to $x_{aug} = [x_{rh}, x_{lh}, \sqrt{x_{rh}^2 + x_{lh}^2}, x_{rk}, x_{lk}, \sqrt{x_{rk}^2 + x_{lk}^2}, x_{ra}, x_{la}, \sqrt{x_{ra}^2 + x_{la}^2}]$. For simplicity, x will be used in place of x_{aug} in this thesis whenever it is clearly multiplied by H.

H is then the least squares solution to

$$HX_{aug} = Y, \tag{2.13}$$

where X_{aug} is the entire augmented dataset of X. As with F, the ridge regression was used to estimate H:

$$H = YX_{aug}^T(X_{aug}X_{aug}^T + \lambda_H I)^{-1}, \tag{2.14}$$

where $\lambda_H = 1$ is the ridge regression parameter optimized during offline pilot testing.

The noise covariance matrix R was estimated using

$$R = \frac{E_H E_H^T}{T - d_2}, \tag{2.15}$$

where E_H is the $d_2 \times T$ residual matrix from fitting H

$$E_H = Y - HX_{aug}. \tag{2.16}$$

Recursive Update

In real-time applications, a Kalman filter starts with estimating the current state at time t:

$$x_{t'} = Fx_{t-1} \tag{2.17}$$

and

$$P_{t'} = FP_{t-1}F^T + Q, \tag{2.18}$$

where $x_{t'}$ and $P_{t'}$ are the predicted state and its covariance; x_{t-1} and P_{t-1} are the previous state and its covariance.

In the update step, the current EEG z_t is predicted from $x_{t'}$:

$$y_t = Hx_{t'}. \tag{2.19}$$

The difference between the predicted EEG signal y_t and observed EEG z_t is used to correct the predicted $x_{t'}$ to better correspond to the observation. This correction first requires calculating a matrix S, the covariance that describes the uncertainty in the predicted EEG:

$$S_t = HP_{t'}H^T + R. \tag{2.20}$$

The amount of correction depends on the uncertainty of the current state estimate and the uncertainty in the prediction. A Kalman gain K_t is used to describe this weighted decision between $x_{t'}$ and z_t, and calculate the final estimation x_t:

$$K_t = P_{t'}H^T S_t^{-1}. \tag{2.21}$$

Lastly, the current x_t and P_t are updated by

$$x_t = x_{t'} + K_t(y_t - z_t) \tag{2.22}$$

and

$$P_t = (I - K_t H) P_{t'}, \tag{2.23}$$

where I is the identity matrix.

Closed-loop Decoder Adaptation

The last bit of detail is the implementation of a closed-loop decoder adaptation (CLDA) [63] algorithm. Under this real-time training paradigm, the EEG and joint angle data were streamed to a buffer. Each minute, the buffered data were used to fit a new set of F, H, Q, and R. Once a new set was fitted, these matrices were updated by taking a weighted sum of the new values and the values from the previous update.

CLDA was activated in the training phase and deactivated in the testing phase. As a result, the UKF decoder was updated every minute during the testing phase, and then kept fixed during the testing phase. This practice has two advantages: 1) after the 10-minute training, the decoder was fixed. This avoids overfitting as it is "cheating" for the decoder to keep adapting during testing; 2) it allows the decoder to function and produce output during the training phase, starting from as early as the second minute.

2.6 Offline Preprocessing

The procedures described so far were all implemented during data collection. The data were subsequently processed offline for further analysis. The offline processing consists of three parts: artifact subspace reconstruction (ASR) on EEG data, gait segmentation, and EEG power analysis in frequency domain.

ASR was applied to remove EEG artifacts that are detectable in the time domain (e.g., eye blinks, EMG burst). ASR applies principal component analysis to the EEG data in sliding windows and identifies channels that significantly deviate from the baseline data containing minimal movement artifact. Channels with variance above a predefined

threshold compared to the baseline data are identified as corrupted and reconstructed using a mixing matrix that is computed from the baseline data. The EEG data during the standing phase in each trial were used as baseline [64, 44]. Default parameters in the Matlab plugin clean-rawdata were applied.

The rest of the offline processing was performed with Python. Here is a list of the open source Python packages used in this dissertation: numpy, scipy, matplotlib, scikit-learn, mne, jupyter, seaborn, keras, tensorflow, and statsmodels.

Both EEG and goniometer data were subsequently segmented into gait cycles based on the right knee joint of the subjects. Knee joint angle has an easy-to-identify spike in the swing phase. Peak flexion of the knee happens mid swing phase. The right knee was preferred over the left because it is the unaffected side of all subjects, which generally has more stable kinematics profile. Note that gait cycles are usually defined as the interval between two heel contact on the same foot using foot switches [65]. For the purpose of this dissertation, the onset of gait cycle is not relevant. After the joint angles were segmented into gait cycles, the accompanying EEG data were segmented accordingly.

Chapter 3

Neural Decoding

3.1 Metrics

The decoder performance in each gait cycle was assessed by the Pearsons correlation coefficient r between the measured and predicted joint angles on the affected leg (the brain-controlled leg on avatar). $r = 1$ would indicate that the measured and predicted data are the same (except from scale). $r = 0$ indicates the two signals are uncorrelated. With the r values, the decoder performance within each gait cycle was quantified by a scalar. The average performance of a trial is defined as the median of r among all gait cycles.

Note that the ankle joint angles were recorded and decoded, but not included in further analysis because some subjects had very limited range of motion on their left ankle. S3 could not voluntarily flex his left ankle at all. Results showed that the performance on hip and knee joints were very close. For this reason, the r from left (affected side) hip joint was chosen as the main metric when evaluating decoder performance.

3.2 Results

Firstly, goniometer and EEG data were segmented into gait cycles. Figure 3.1 shows an example of the gait segmentation based on peaks in the right knee profile in S1. Gait events (maximum knee flexion) were accurately registered.

Figure 3.2 shows the decoder performance on the left hip of all subjects. Data were aggregated across all trials (S1: 16 trials, S2: 14 trials, S3: 13 trials). Each dot

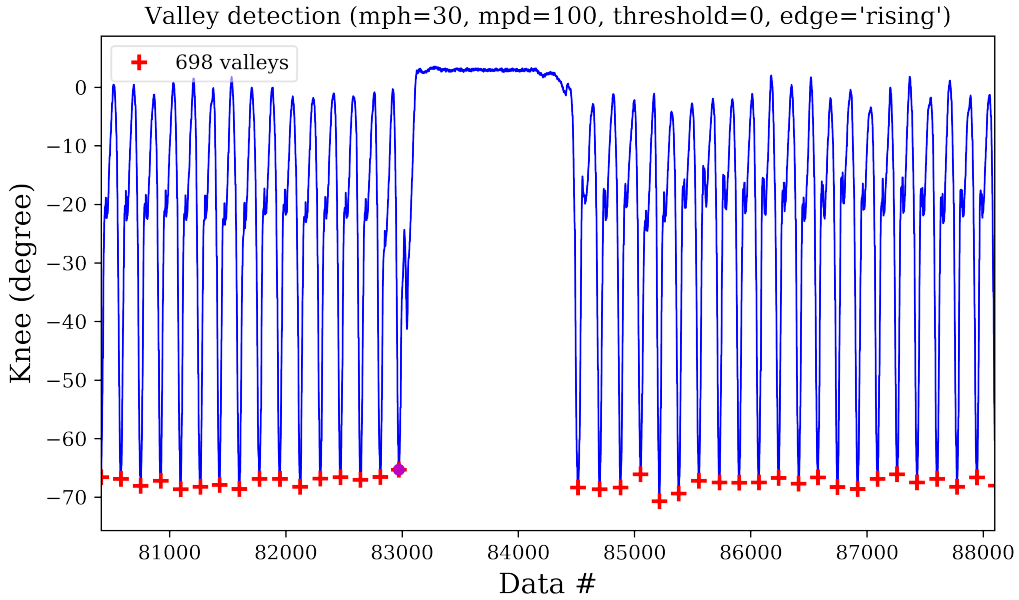

Figure 3.1: Automatic gait segmentation based on the right knee joint angle measured by goniometer. Each cross marks a gait that was identified by the algorithm.

represents the decoder performance r in one gait cycle. The distribution of r for each subject is shown on the right. There are several interesting patterns to be observed: 1) r was evenly distributed across the whole range between -1 and 1 in the beginning, then converged as the decoder updated; 2) the performance in the first 10 minutes was slightly better than the second 10 minutes because the decoder stopped updating in the second 10 minutes, namely the *testing* phase; 3) the r distribution was non-Gaussian, biased towards the higher direction. These phenomena are expected from the study design, validating the correctness of the results.

The three distributions on the right side of Figure 3.2 was further aggregated into one histogram (Figure 3.3). The mode of the distribution (peak density) occurred at $r = 0.83$. The distribution is non-Gaussian. It is therefore better to describe the average performance with median which will be discussed next.

The average performance in each trial is the median r among all gait cycles. Figure 3.4 shows this metric against time. The performance was relatively stable among

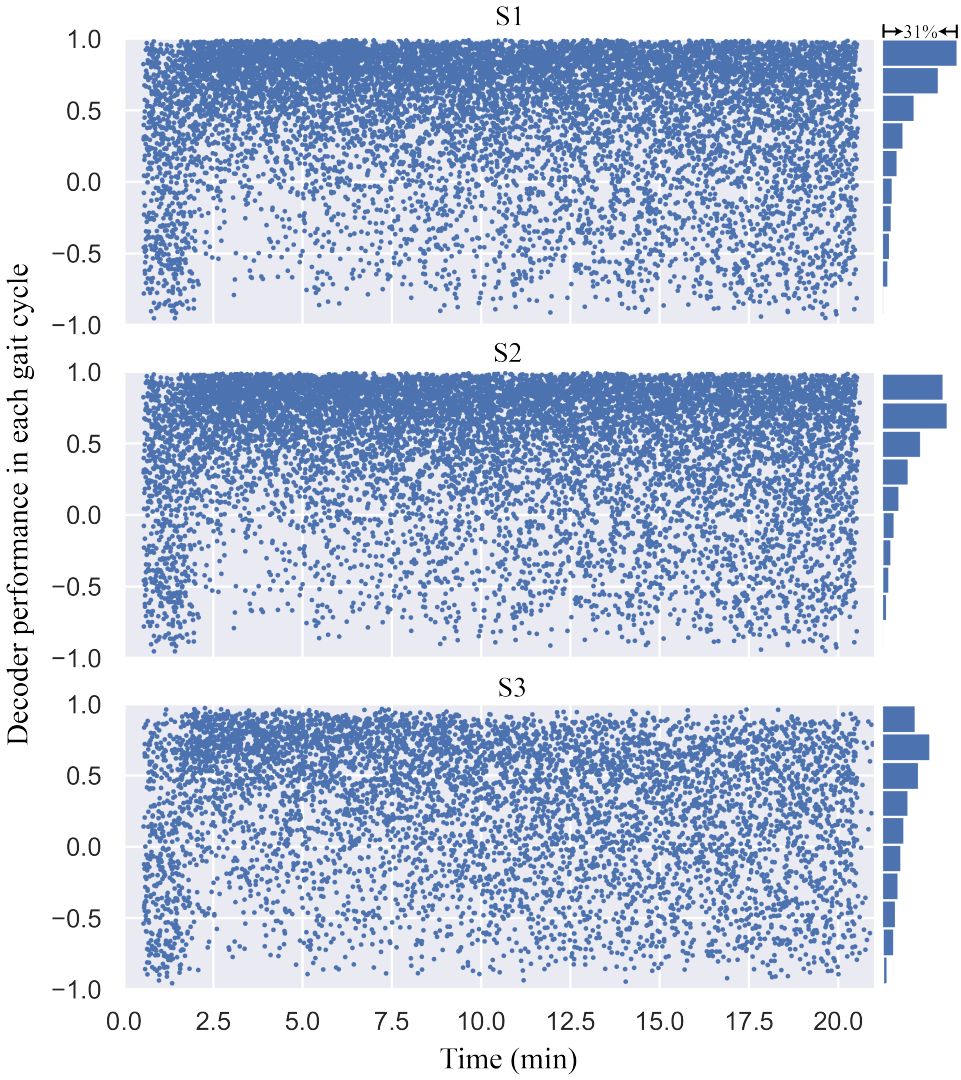

Figure 3.2: Decoder performance in each gait cycle. Each panel represents a subject. Each dot represents the decoder performance in one gait cycle. The distribution aggregated over all trials is shown on the right.

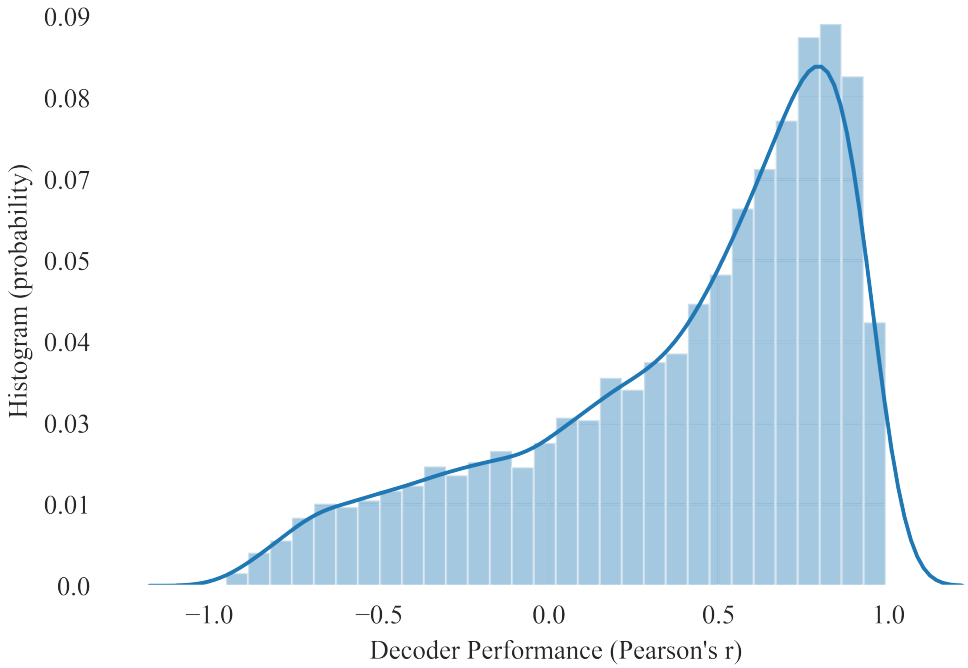

Figure 3.3: Histogram of the decoder performance across all subjects and trials. The peak occurs at $r = 0.83$.

each subject. Interestingly, significant inter-subject performance differences exist, which will be further discussed. Averaged across trials, the r from S1, S2, and S3 were 0.60, 0.59, 0.30 respectively. The mean r across subjects was 0.50.

3.3 Discussion

The performance reported above is comparable, and better in some cases, to previous literature. A study using offline decoding with stroke survivors using exoskeletons reported $r = 0.61$ [43]. However, it utilized processing methods that are not available in real-time, such as principle component analysis (PCA). Surprisingly, the present result is better than the performance from 8 healthy subjects ($r = 0.42$) in our previous publication [44]. There are a couple of improvements in data collection methods since then that may have contributed to the better performance.

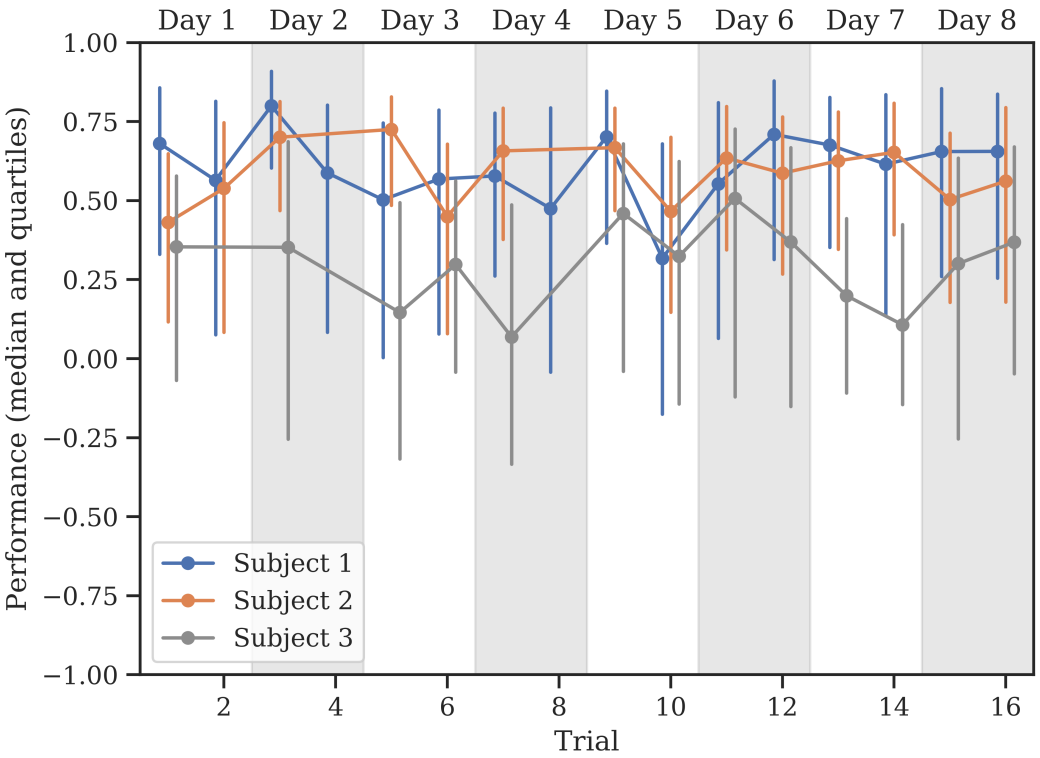

Figure 3.4: Median decoder performance (r value) of the left hip joint. There were two trials each day, which is illustrated by the white/grey shaded area. The vertical bars indicate the 25th and 75th percentile distribution.

1) EEG electrode impedance was maintained mostly below 20 kΩ with S1 and S2 (who had better performance), and around 40 kΩ with S3. In the previous study, impedance was only kept below 60 kΩ.

2) Subjects in the present study wore an elastic mesh wrapping around the EEG cap to reduce the motion and displacement of the sensors and cables.

There are not enough data to validate if these factors directly contribute to decoder performance, nor to prove that there is statistically significant performance between the two studies.

No significant performance improvement was observed across sessions. This differs from the results from previous studies [55, 66]. The difference likely comes from the difference in their protocols. The subjects in [66], who were all healthy subjects, were

given minimal instructions and encouraged to freely explore movements and strategies during BCI controls and visual-motor perturbations. As an example, the subject had to first figure out which leg was controlled by the EEG. Participants in the present study received more explanations about the protocols, reducing the extent of learning. This is because the present study focuses more on the effect of BCI rather than motor exploration. The end effector of the BCI in [55] is a powered wearable exoskeleton. The physical challenge for stroke survivors to walk in an exoskeleton was considerable. They were likely to have highly irregular kinematics in early sessions. This might explain the improved decoder performance over time.

Chapter 4

Cortical Plasticity

4.1 Metrics

Welch's method was used to compute the power spectral density (PSD) of each remaining EEG channel after artifact removal. The power in five common frequency bands (delta (0.1–4 Hz), theta (4–7 Hz), alpha (7–12 Hz), beta (12–25 Hz), and low gamma (25–50 Hz)) were calculated respectively. Additionally, EEG recorded during the training and testing phases were computed separately for comparison. Because each EEG channel has its own frequency characteristics, the above power analysis was performed for each channel individually.

A strong relationship between an EEG frequency content and the decoder performance r in certain channels would suggest this frequency content is related with the task. Therefore, linear regression between the r and frequency contents at each EEG channel was attempted across all gait cycles in each trial. The likelihood of their dependency (not the strength of dependency) in that trial was measured by the p value of the regression.

4.2 Results

Decoder performance was found to correlate to the delta band EEG power in many channels. However, some of them may be the result of "p farming". There are 60 channels $\times$ 5 frequency bands $\times$ 6 joints = 1800 features to be regressed with the r value. It is possible that some of those features have a distribution that match the r only out of chance. In fact, occasional "significant" channels were indeed found in other bands. To overcome this limitation, for each channel I examined how many trials demonstrated

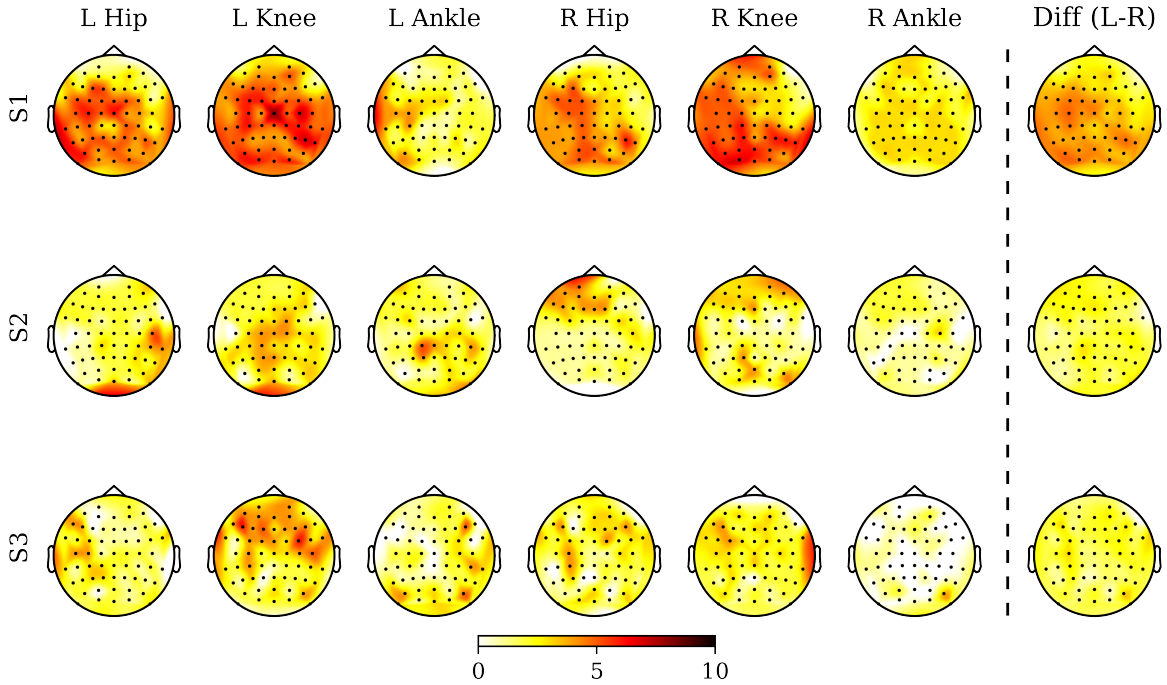

Figure 4.1: The number of trials in which a significant correlation was found between the decoder performance and delta band power across gait cycles. The difference between those numbers on the left and right side, averaged across joints, is shown in the last column.

statistical significance. The underlying assumption is that if a significant relationship was observed in multiple trials, it is more likely to be true. Figure 4.1 shows the number of trials that showed significant relationship between delta band EEG and r for each channel. It demonstrates that 1) delta band power was significantly related with BCI performance, especially in Subject 1, who had the best performance; 2) delta band power was correlated with the joints on the left side more than the right side, which is expected because the BCI task was to control the left leg.

Figure 4.2 shows interesting patterns in the delta band power between the training and testing phases. The power in the testing phase was statistically lower than that in the training phase (two-sided t-test $p = 0.0487$). Although this difference was not significant in S2, it significantly increased over trials (linear regression $p = 0.0174$). S3 did not show any noticeable pattern, possibly correlated to his low decoder performance. A steady increase in the theta band power was observed across trials in S1 (Figure 4.3).

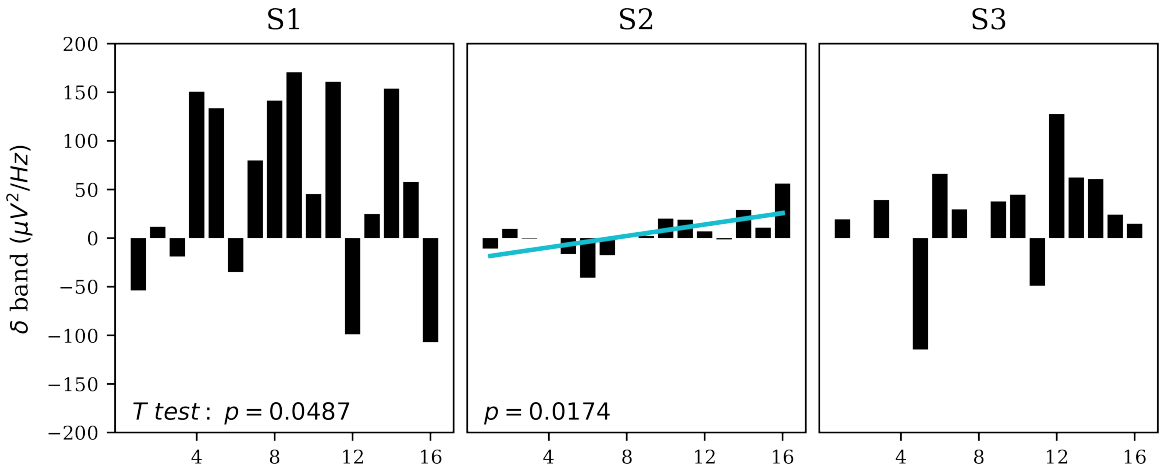

Figure 4.2: The difference between the training and testing phase in the power of delta band in all subjects and all trials. The x axis represents the trial index.

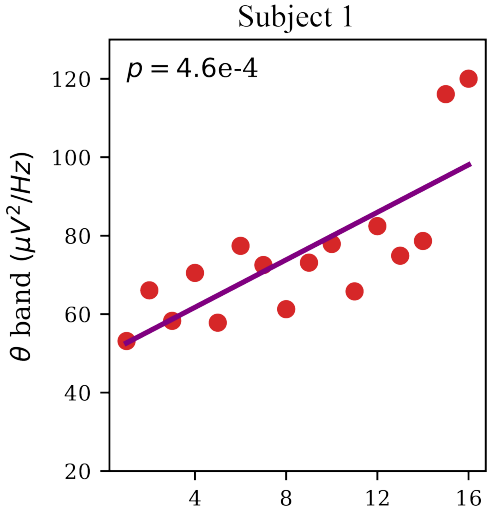

Figure 4.3: Theta band power increased over trials in S1. The x axis represents the trial index.

4.3 Discussion

Delta band EEG is the driving feature in the present BCI design. It was first reported to be associated with walking in [67, 68]. Our group has explored this feature in a series of previous BCI studies with healthy subjects [69, 70, 54, 59]. Delta band was tested in two studies with stroke survivors who tried out lower-limb exoskeletons [43, 55]. They were both offline and heavily involved exoskeletons in their protocols. The present study is the first one to explore how delta band EEG is related with the

decoder performance in human walking.

Theta band power is not usually associated with motor learning in previous literature. Theta power increase in the sensorimotor area after differential learning (DL) of motor skills was reported in [71]. DL is a self-organized learning process in which the learner will find an individually optimized solution for a movement problem and practice each element of this to-be-learned movement.

Because of the small sample size and limited session number, it is unclear if the observed cortical adaptation would remain after a prolonged period of time. The mechanism of BCI-triggered cortical plasticity is an active research subject that certainly needs more study in the future [72].

Chapter 5

Motor Adaptation

5.1 Metrics

The consistency in subjects' kinematics is expected to improve over trials as the subjects become familiar with the protocol. Two metrics were developed to measure this consistency in the temporal and spatial domain respectively.

The *temporal gait consistency score* is defined as the standard deviation (SD) of the duration of all gaits in each trial. The smaller the deviation is, the more consistent the subject walks.

The *spatial gait consistency score* is defined as the SD of the position of the centroid of each gait trajectory. The definition of a gait trajectory and its centroid are given below. Gait trajectory is the movement of the foot in the sagittal plane, or the plane of progression, during one gait cycle. It can be estimated by forward kinematics, combining the length of shank and thigh, and joint angles at hip and knee (Figure 5.1). Because of its repetitive nature, each gait trajectory forms an enclosed 2D shape. Centroid of this shape was used to describe spatial variation over time.

A centroid of a shape, also known as the center of mass, (C_x, C_y), is the arithmetic mean position of all the points in that shape. The centroid of a 2-dimensional n-point polygon with vertices $[x_i, y_i]$, $(i = 1, 2, ..., n)$ is

$$C_x = \frac{1}{6A} \sum_{i=0}^{n-1} (x_i + x_{i+1})(x_i y_{i+1} - x_{i+1} y_i) \tag{5.1}$$

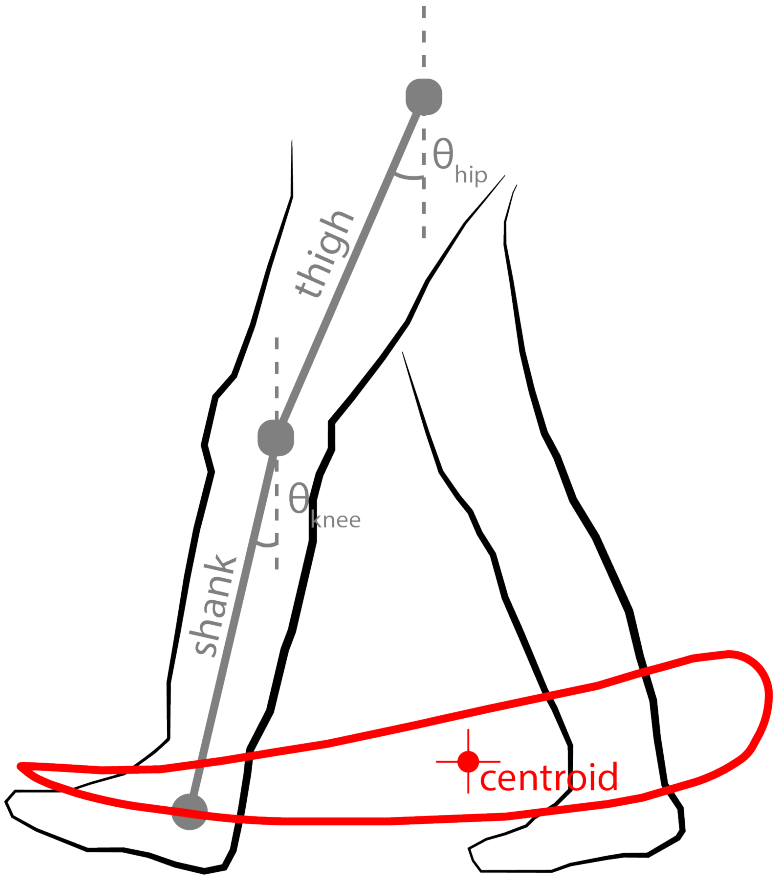

Figure 5.1: Forward kinematics and centroid of gait trajectory. The gait trajectory was estimated by calculating the foot's sagittal position based on joint angles and limb length. A centroid can then be found for this trajectory.

and

$$C_y = \frac{1}{6A}\sum_{i=0}^{n-1}(y_i + y_{i+1})(x_i y_{i+1} - x_{i+1}y_i), \tag{5.2}$$

where A is the polygon's signed area, as described by

$$A = \frac{1}{2}\sum_{i=0}^{n-1}(x_i y_{i+1} - x_{i+1}y_i). \tag{5.3}$$

Figure 5.1 illustrates a typical foot trajectory and its centroid. The spatial consistency score measures gait cycles' spatial variation by tracing how the centroid moves across gaits. A small consistency score indicates stable walking pattern.

The third metric in use was the *bilateral symmetry score* between the range of

motion (ROM) of left and right hip joints. The ROM in each gait cycle is defined as the difference between maximum and minimum joint angles. From there, the definition of symmetry is straightforward:

$$Symmetry = \frac{ROM_{right} - ROM_{left}}{ROM_{right} + ROM_{left}}. \tag{5.4}$$

For healthy humans who walk symmetrically, this score would be close to zero.

5.2 Results

Figure 5.2 shows the temporal gait consistency score of all subjects. The score was measured by the SD of the gait duration in each trial. The smaller the SD of this time is, the more consistently the subject walked during that trial, which indicates that the subject was more skilled and confident at the task. Because of the non-negative nature of SD, it would eventually reach a plateau given enough trials or practices. A significant decrease of the variation over trials was observed in S1 and S3. The score in each subject was normalized and aggregated, forming the bottom right panel in the figure. The same decreasing trend was significant across subjects.

Figure 5.3 shows the spatial gait consistency score of S1, whose variation significantly decreased over trials. The variation in S2 and S3 did not change significantly in any direction.

Figure 5.4 shows the bilateral symmetry score (defined in Eq. 5.4) in each joint (hip, knee, and ankle) for each subject across trials. No particular trend was observed in S1 and S3, but S2 showed statistically significant convergence towards the neutral level (score of 0) in his knee and ankle.

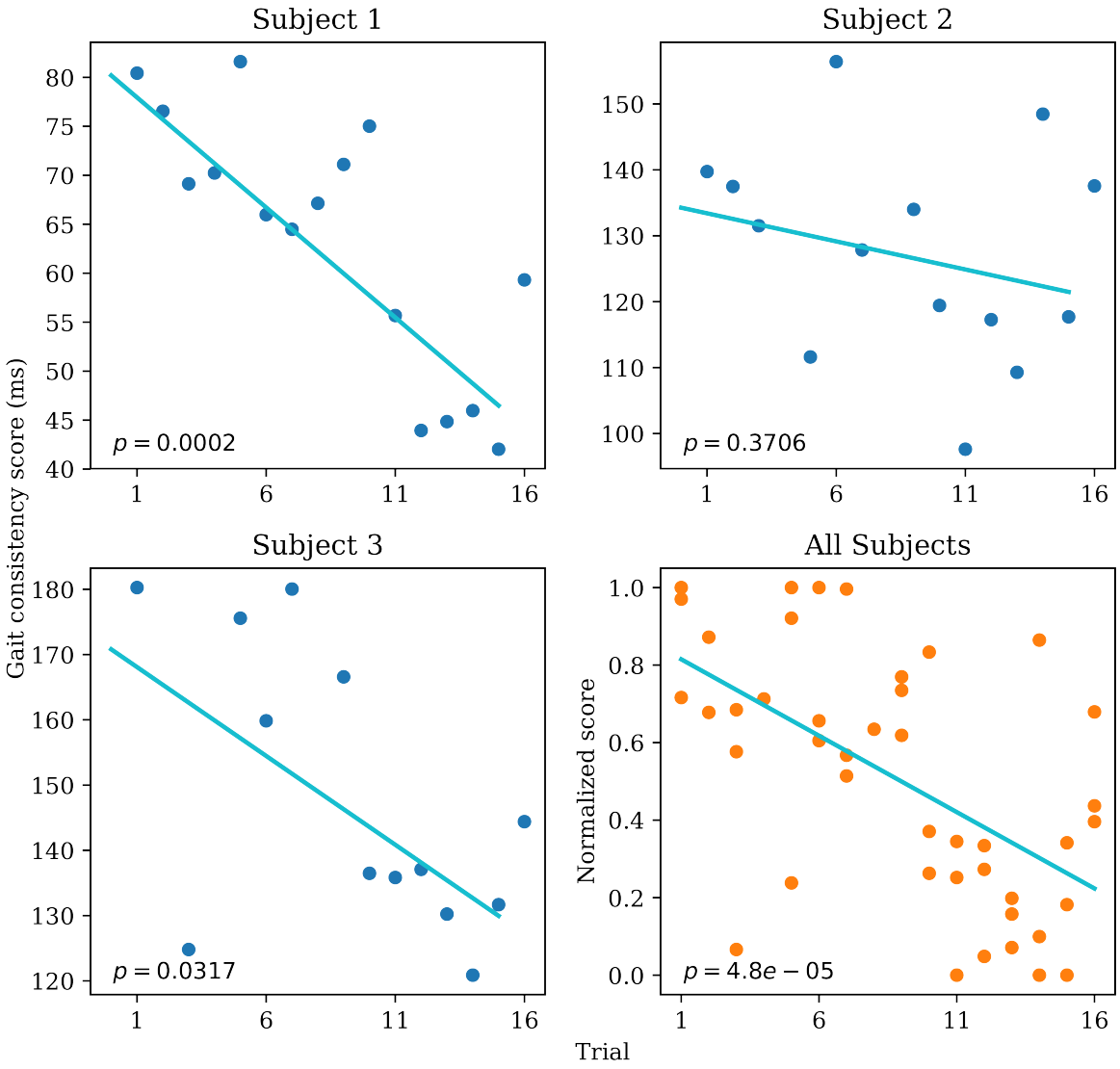

Figure 5.2: The temporal gait consistency score (standard deviation of the duration of each gait) decreases over trials, suggesting that the subjects learned to walk in more consistent manner.

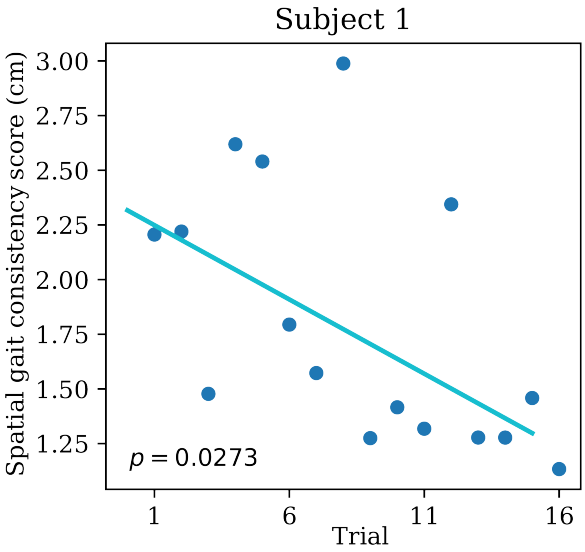

Figure 5.3: The spatial gait consistency score (variation of the centroid of the heel trajectory in each gait) decreases over trials in Subject 1.

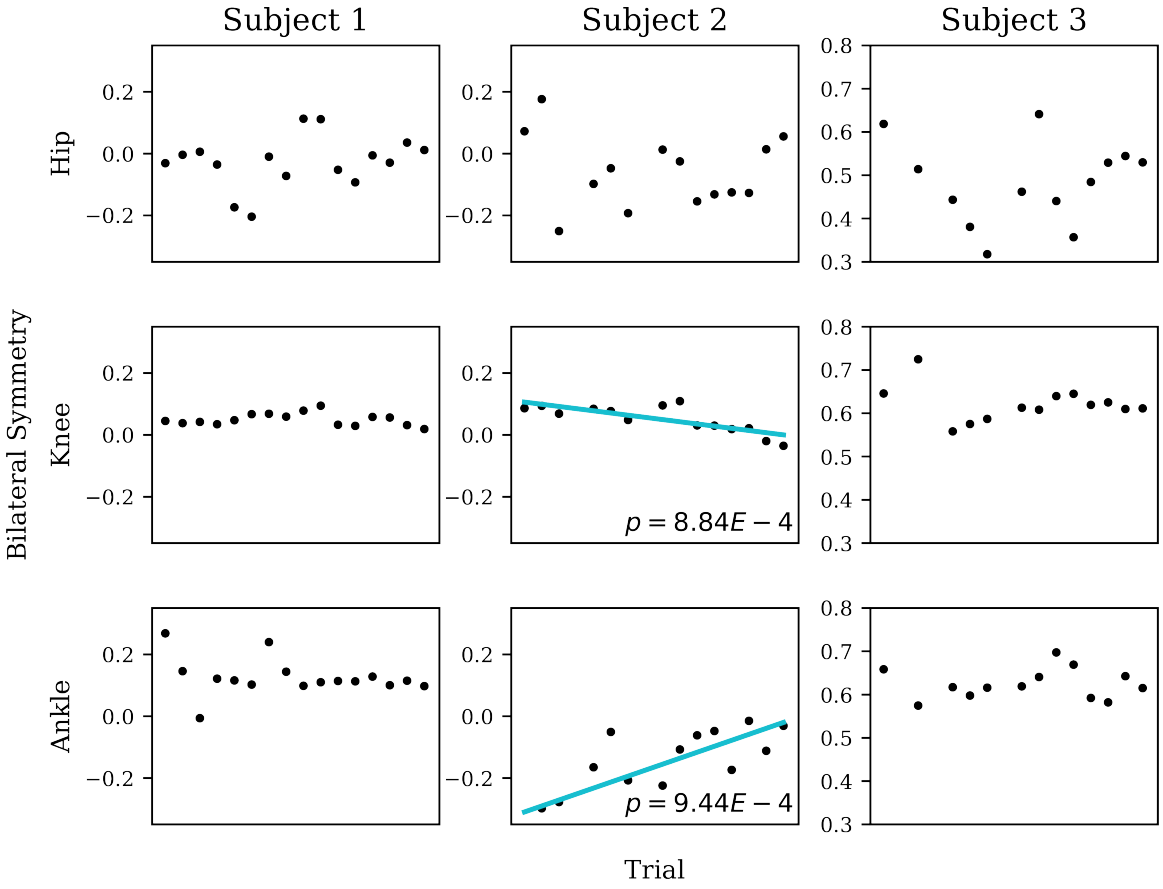

Figure 5.4: The bilateral symmetry score in all joints across trials. Subject 2 knee and ankle joints showed a statistically significant trend towards the neural score of 0.

5.3 Discussion

These kinematics metrics, inspired by human kinematics, have a few advantages over clinical benchmarks such as the 10-meter Walk, 6-min Walk, and Timed Up and Go test in the context of this study. Firstly, they are completely transparent to the subjects, adding no additional physical or mental burden. Secondly and subsequently, they do not increase the time needed in the experiment. Thirdly, they allow constant and real-time monitoring. For example, a gait consistency score could be calculated for each gait cycle, revealing intra-trial patterns. This is not practical with most other clinical assessments.

The gait consistency scores are useful in stroke rehabilitation because they quantitatively measure the progress of motor learning of the patients. This is especially true if the goal is to use innovative methods to trigger plasticity. Plateau of the scores is one indicator that the amount of learning and improving in this patient is becoming marginal.

Subject 2's improvement in bilateral symmetry score is especially promising. Anecdotally, S2 expressed a strong belief that his gait posture has improved. This improvement possibly results from the visual feedback of his imbalanced gait during the training phase. Visual feedback has long been used in stroke rehabilitation in the form of mirror therapy [73, 74, 75]. With recent developments in virtual reality and augmented reality, the boundary will likely be pushed forward on this front [76, 77].

Chapter 6

Conclusion

6.1 Future Directions

This dissertation contributes to the advancement of stroke rehabilitation in two ways. First, it provides evidence that BCI could be used in the task of lower limb control for the stroke population. This discovery opens a brand new field of exploration in the stroke rehabilitation research. Secondly, it suggests EEG could evaluate progress in stroke rehabilitation and motor training. This dissertation serves as a pilot study, paving the path for future clinical trials to continue answering these questions with more rigorous experiment designs.

Specifically, the experiment can be improved by adding control groups. The control groups may take form in 1) limited-treatment, where the subjects just walk on a treadmill for the same duration as in the present study; 2) sham group, where the subject controls an avatar to walk in TV without any BCIs.

Both control groups address interesting underlying questions. The conventional clinical wisdom says that the potential for recovery in chronic stage of stoke is significantly diminished [12]. Therefore no recovery is expected from the limited-treatment group. However, this view was challenged by a meta-analysis providing evidence for stroke rehabilitation even in this stage [78]. Most of the research on this topic are related to motor functions in the upper limb. As there is no consensus established for the lower limb, this control group is necessary to demonstrate the possible advantage of the presented methods.

The scam group is also of particular interest. A meta review found weak evidence

that virtual reality plays a positive role in stroke rehabilitation [79]. The virtual environment in the present study is similar to a mirror therapy where the patient looks into a mirror while performing physical actions [75]. The difference is that the avatar in the present study was placed at the same point of view as the patient (facing the same direction), therefore likely to elicit a stronger sense of embodiment. However, there is no solid evidence of whether or how much improvement can be achieved. A sham group without BCI would separate the effects from virtual reality and BCI. Note that it is not possible to design a sham group with closed-loop BCI but without using virtual reality or any other novel techniques, because the BCI result needs to be conveyed to the subject eventually.

Other clinical limitations in the current study include the small number of subjects and heterogeneity of their stroke location. Three subjects are an ideal size for a pilot trial of the proposed novel method, but not enough as a clinical cohort. Furthermore, there are both cortical and sub-cortical cases of stroke among the three subjects, which is better to be controlled in future studies.

There are also questions unanswered in the algorithm design. Currently, a single treadmill speed was set throughout each session, making the movement of the subject rather predicable. Although this knowledge of periodic movement was not used in the decoder design, ultimately it would be more useful if the decoder was able to adapt to changing speed.

Another limitation in the current algorithm is its assumption of the stationary system. Eq. 2.7 and Eq. 2.8 are only valid if 1) the Markov chain governing the hidden states (joint angles), F, does not change over time; 2) the relationship between EEG and hidden states, H, does not change; 3) the noise term Q and R do not change. Among these assumptions, it is reasonably safe to consider F static because the subjects walked in consistent manners. However, there was no guarantee that H, Q, and R are time-

invariant. The current decoder, which was individually trained in every trial, performs poorly if transferred to other trials. Better mathematical models or engineering tools may further enhance the decoder to reduce the need of retraining.

6.2 Summary

This dissertation presents a real-time BCI for chronic stroke survivors for their gait rehabilitation, which is the first of its kind in current literature. Three Specific Aims were proposed to thoroughly characterize the effect of such a BCI: 1) real-time neural decoding during walking; 2) identifying neural changes during the BCI task; 3) and identifying motor learning during the BCI task.

For the first Aim, results show that decent performance was achieved ($r = 0.60$, 0.59, 0.30 for the three subjects, averaged at 0.50). This is comparable, and in some cases better, than previous literature with healthy subjects or offline decoding. For the second Aim, the delta band EEG which drives the BCI decoder, was found to have significantly difference during BCI control. By introducing the regression between decoder performance r and the delta power, their correlation is quantitatively shown for the first time. For the third Aim, several interesting motor learning effects was observed across trials. Spatial and temporal gait consistency improved in some subjects over trials. Bilateral symmetry in gait patterns was significantly improved in Subject 2.

These results suggest that the presented EEG-based BCI with stroke survivors is a promising tool for their rehabilitation. This information is valuable to advance our knowledge about changes in EEG and BCI performance in the context of stroke rehabilitation.

References

[1] A. C. Zemke, P. J. Heagerty, C. Lee, and S. C. Cramer, "Motor cortex organization after stroke is related to side of stroke and level of recovery," *Stroke*, vol. 34, no. 5, pp. e23–e26 2003.

[2] F. B. van Meulen, D. Weenk, E. H. F. van Asseldonk, H. M. Schepers, P. H. Veltink, and J. H. Buurke, "Analysis of balance during functional walking in stroke survivors," *PLoS ONE*, vol. 11, no. 11, p. e0166789 2016.

[3] P. Langhorne, J. Bernhardt, and G. Kwakkel, "Stroke rehabilitation," *The Lancet*, vol. 377, no. 9778, pp. 1693–1702 2011.

[4] A. J. Orrell, F. F. Eves, and R. S. W. Masters, "Motor learning of a dynamic balancing task after stroke: implicit implications for stroke rehabilitation," *Physical Therapy*, vol. 86, no. 3, pp. 369–380 2006.

[5] A. Kaelin-Lang, "Role of voluntary drive in encoding an elementary motor memory," *Journal of Neurophysiology*, vol. 93, no. 2, pp. 1099–1103 2004.

[6] M. Lotze, "Motor learning elicited by voluntary drive," *Brain*, vol. 126, no. 4, pp. 866–872 2003.

[7] E. Olgiati, C. Russell, D. Soto, and P. Malhotra, "Motivation and attention following hemispheric stroke," *Progress in Brain Research*, vol. 229, pp. 343–366 2016.

[8] S. H. Collins and R. W. Jackson, "Inducing self-selected human engagement in robotic locomotion training," *IEEE International Conference on Rehabilitation Robotics* 2013.

[9] A. Koenig, X. Omlin, L. Zimmerli, M. Sapa, C. Krewer, M. Bolliger, F. Müller, and R. Riener, "Psychological state estimation from physiological recordings during robot-assisted gait rehabilitation," *Journal of Rehabilitation Research and Development*, vol. 48, no. 4, pp. 367–85 2011.

[10] F. Grimm, G. Naros, and A. Gharabaghi, "Closed-loop task difficulty adaptation during virtual reality reach-to-grasp training assisted with an exoskeleton for stroke rehabilitation," *Frontiers in Neuroscience*, vol. 10, no. November, p. 518 2016.

[11] P. Raghavan, D. Geller, N. Guerrero, V. Aluru, J. P. Eimicke, J. A. Teresi, G. Ogedegbe, A. Palumbo, and A. Turry, "Music upper limb therapy-integrated: an enriched collaborative approach for stroke rehabilitation," *Frontiers in Human Neuroscienceuman Neuroscience*, vol. 10, no. October, p. 498 2016.

[12] S. R. Soekadar, N. Birbaumer, M. W. Slutzky, and L. G. Cohen, "Brain-machine interfaces in neurorehabilitation of stroke," *Neurobiology of Disease*, vol. 83, pp. 172–179 2015.

[13] J. M. Carmena, M. A. Lebedev, R. E. Crist, J. E. O'Doherty, D. M. Santucci, D. F. Dimitrov, P. G. Patil, C. S. Henriquez, and M. a. L. Nicolelis, "Learning to control a brain-machine interface for reaching and grasping by primates," *PLoS Biology*, vol. 1, no. 2, p. e42 2003.

[14] K. Ganguly and J. M. Carmena, "Emergence of a stable cortical map for neuroprosthetic control," *PLoS Biology*, vol. 7, no. 7, p. e1000153 2009.

[15] L. R. Hochberg, D. Bacher, B. Jarosiewicz, N. Y. Masse, J. D. Simeral, J. Vogel, S. Haddadin, J. Liu, S. S. Cash, P. van der Smagt, and J. P. Donoghue, "Reach and grasp by people with tetraplegia using a neurally controlled robotic arm," *Nature*, vol. 485, no. 7398, pp. 372–375 2012.

[16] J. L. Collinger, B. Wodlinger, J. E. Downey, W. Wang, E. C. Tyler-Kabara, D. J. Weber, A. J. McMorland, M. Velliste, M. L. Boninger, and A. B. Schwartz, "High-performance neuroprosthetic control by an individual with tetraplegia," *The Lancet*, vol. 381, no. 9866, pp. 557–564 2013.

[17] C. E. Bouton, A. Shaikhouni, N. V. Annetta, M. A. Bockbrader, D. A. Friedenberg, D. M. Nielson, G. Sharma, P. B. Sederberg, B. C. Glenn, W. J. Mysiw, A. G. Morgan, M. Deogaonkar, and A. R. Rezai, "Restoring cortical control of functional movement in a human with quadriplegia," *Nature*, vol. 533, no. 7602, pp. 247–250 2016.

[18] J. A. Perge, M. L. Homer, W. Q. Malik, S. Cash, E. Eskandar, G. Friehs, J. P. Donoghue, and L. R. Hochberg, "Intra-day signal instabilities affect decoding performance in an intracortical neural interface system," *Journal of Neural Engineering*, vol. 10, no. 3, p. 036004 2013.

[19] J. Meng, S. Zhang, A. Bekyo, J. Olsoe, B. Baxter, and B. He, "Noninvasive electroencephalogram based control of a robotic arm for reach and grasp tasks," *Scientific Reports*, vol. 6, no. December, p. 38565 2016.

[20] Y. He, D. Eguren, J. Azorín, R. Grossman, T. P. Luu, and J. L. Contreras-Vidal, "Brain-machine interfaces for controlling lower-limb powered robotic systems," *Journal of Neural Engineering*, vol. 15, no. 2, p. 021004 2018.

[21] T. Ono, A. Kimura, and J. Ushiba, "Daily training with realistic visual feedback improves reproducibility of event-related desynchronisation following hand motor imagery," *Clinical Neurophysiology*, vol. 124, no. 9, pp. 1779–1786 2013.

[22] E. Buch, C. Weber, L. G. Cohen, C. Braun, M. A. Dimyan, T. Ard, J. Mellinger, A. Caria, S. Soekadar, A. Fourkas, and N. Birbaumer, "Think to move: a

neuromagnetic brain-computer interface (BCI) system for chronic stroke," *Stroke*, vol. 39, no. 3, pp. 910–917 2008.

[23] N. A. Bhagat, A. Venkatakrishnan, B. Abibullaev, E. J. Artz, N. Yozbatiran, A. A. Blank, J. French, C. Karmonik, R. G. Grossman, M. K. O'Malley, G. E. Francisco, and J. L. Contreras-Vidal, "Design and optimization of an EEG-based brain machine interface (BMI) to an upper-limb exoskeleton for stroke survivors," *Frontiers in Neuroscience*, vol. 10, no. March, p. 122 2016.

[24] K. Kim, H. Suk, and S. Lee, "Commanding a brain-controlled wheelchair using steady-state somatosensory evoked potentials," *IEEE Transactions on Neural Systems and Rehabilitation Engineering*, vol. 26, no. 3, pp. 654–665 2016.

[25] A. Fernández-Rodríguez, F. Velasco-Álvarez, and R. Ron-Angevin, "Review of real brain-controlled wheelchairs," *Journal of Neural Engineering*, vol. 13, no. 6, p. 061001 2016.

[26] F. Galán, M. Nuttin, E. Lew, P. Ferrez, G. Vanacker, J. Philips, and J. d. R. Millán, "A brain-actuated wheelchair: asynchronous and non-invasive braincomputer interfaces for continuous control of robots," *Clinical Neurophysiology*, vol. 119, no. 9, pp. 2159–2169 2008.

[27] M. Seeber, R. Scherer, and J. Wagner, "Spatial-spectral identification of μ and β EEG rhythm sources during robot-assisted walking," *Biomedical Engineering*, vol. 58, pp. 1–2 2013.

[28] M. Seeber, R. Scherer, J. Wagner, T. Solis-Escalante, G. R. Müller-Putz, C. Trenado, M. Seeber, R. Scherer, J. Wagner, T. Solis-Escalante, and G. R. Muller-Putz, "EEG beta suppression and low gamma modulation are different elements of human upright walking," *Frontiers in Human Neuroscience*, vol. 9, no. July, pp. 1–9 2015.

[29] M. Seeber, R. Scherer, J. Wagner, T. Solis-Escalante, and G. R. Müller-Putz, "High and low gamma EEG oscillations in central sensorimotor areas are conversely modulated during the human gait cycle," *NeuroImage*, vol. 112, pp. 318–326 2015.

[30] J. Wagner, S. Makeig, M. Gola, C. Neuper, and G. Muller-Putz, "Distinct band oscillatory networks subserving motor and cognitive control during gait adaptation," *Journal of Neuroscience*, vol. 36, no. 7, pp. 2212–2226 2016.

[31] S. Debener, F. Minow, R. Emkes, K. Gandras, and M. de Vos, "How about taking a low-cost, small, and wireless EEG for a walk?" *Psychophysiology*, vol. 49, no. 11, pp. 1449–53 2012.

[32] S. Finnigan and M. J. van Putten, "EEG in ischaemic stroke: Quantitative EEG can uniquely inform (sub-)acute prognoses and clinical management," *Clinical Neurophysiology*, vol. 124, no. 1, pp. 10–19 2013.

[33] A. I. Sburlea, L. Montesano, R. C. de la Cuerda, I. M. Alguacil Diego, J. C. Miangolarra-Page, and J. Minguez, "Detecting intention to walk in stroke patients from pre-movement EEG correlates," *Journal of NeuroEngineering and Rehabilitation*, vol. 12, no. 1, p. 113 2015.

[34] A. Costa, R. Salazar-Varas, A. Úbeda, and J. M. Azorín, "Characterization of artifacts produced by gel displacement on non-invasive brain-machine interfaces during ambulation," *Frontiers in Neuroscience*, vol. 10, no. Feburary, pp. 1–14 2016.

[35] J. T. Gwin, K. Gramann, S. Makeig, and D. P. Ferris, "Removal of movement artifact from high-density eeg recorded during walking and running," *Journal of Neurophysiology*, vol. 103, no. 6, pp. 3526–3534 2010.

[36] T. M. Lau, J. T. Gwin, K. G. McDowell, and D. P. Ferris, "Weighted phase lag index stability as an artifact resistant measure to detect cognitive EEG activity

during locomotion," *Journal of NeuroEngineering and Rehabilitation*, vol. 9, no. 1, p. 47 2012.

[37] Y.-P. Lin, Y. Wang, and T.-P. Jung, "A mobile SSVEP-based brain-computer interface for freely moving humans: the robustness of canonical correlation analysis to motion artifacts," *35th Annual International Conference of the IEEE Engineering in Medicine and Biology Society (EMBC)*, pp. 1350–3 2013.

[38] K. L. Snyder, J. E. Kline, H. J. Huang, and D. P. Ferris, "Independent component analysis of gait-related movement artifact recorded using eeg electrodes during treadmill walking," *Frontiers in Human Neuroscience*, vol. 9, no. December, pp. 1–13 2015.

[39] A. S. Oliveira, B. R. Schlink, W. D. Hairston, P. König, and D. P. Ferris, "Induction and separation of motion artifacts in EEG data using a mobile phantom head device," *Journal of Neural Engineering*, vol. 13, no. 3, p. 036014 2016.

[40] K. Nathan and J. L. Contreras-Vidal, "Negligible motion artifacts in scalp electroencephalography (eeg) during treadmill walking," *Frontiers in Human Neuroscience*, vol. 9, no. January, pp. 1–12 2016.

[41] J. T. Gwin, K. Gramann, S. Makeig, and D. P. Ferris, "Electrocortical activity is coupled to gait cycle phase during treadmill walking," *NeuroImage*, vol. 54, no. 2, pp. 1289–1296 2011.

[42] C. Cevallos, D. Zarka, T. Hoellinger, A. Leroy, B. Dan, and G. Cheron, "Oscillations in the human brain during walking execution, imagination and observation," *Neuropsychologia*, vol. 79, pp. 223–232 2015.

[43] Y. He, K. Nathan, A. Venkatakrishnan, R. Rovekamp, C. Beck, R. Ozdemir, G. E. Francisco, and J. L. Contreras-Vidal, "An integrated neuro-robotic interface for

stroke rehabilitation using the NASA X1 powered lower limb exoskeleton," *36th Annual International Conference of theIEEE Engineering in Medicine and Biology Society (EMBC)*, pp. 3985–8 2014.

[44] T. P. Luu, S. Nakagome, Y. He, and J. L. Contreras-Vidal, "Real-time EEG-based brain-computer interface to a virtual avatar enhances cortical involvement in human treadmill walking," *Scientific Reports*, vol. 7, no. 1, p. 8895 2017.

[45] J. Wagner, T. Solis-Escalante, P. Grieshofer, C. Neuper, G. Müller-Putz, and R. Scherer, "Level of participation in robotic-assisted treadmill walking modulates midline sensorimotor EEG rhythms in able-bodied subjects," *NeuroImage*, vol. 63, no. 3, pp. 1203–1211 2012.

[46] R. Xu, N. Jiang, C. Lin, N. Mrachacz-Kersting, K. Dremstrup, and D. Farina, "Enhanced Low-Latency Detection of Motor Intention From EEG for Closed-Loop Brain-Computer Interface Applications," *IEEE Transactions on Biomedical Engineering*, vol. 61, no. 2, pp. 288–296 2014.

[47] P. T. Wang, C. E. King, L. Chui, A. H. Do, and Z. Nenadic, "Self-paced braincomputer interface control of ambulation in a virtual reality environment," *Journal of Neural Engineering*, vol. 9, no. 5, p. 056016 2012.

[48] C. E. King, P. T. Wang, L. A. Chui, A. H. Do, and Z. Nenadic, "Operation of a brain-computer interface walking simulator for individuals with spinal cord injury," *Journal of Neuroengineering and Rehabilitation*, vol. 10, no. 1, p. 77 2013.

[49] D. Broetz, C. Braun, C. Weber, S. R. Soekadar, A. Caria, and N. Birbaumer, "Combination of brain-computer interface training and goal-directed physical therapy in chronic stroke: a case report," *Neurorehabilitation and Neural Repair*, vol. 24, no. 7, pp. 674–679 2010.

[50] D. J. Leamy, J. J. Kocijan, K. Domijan, J. Duffin, R. A. Roche, S. Commins, R. Collins, and T. E. Ward, "An exploration of EEG features during recovery following stroke - implications for BCI-mediated neurorehabilitation therapy," *Journal of NeuroEngineering and Rehabilitation*, vol. 11, no. 1, p. 9 2014.

[51] E. García-Cossio, M. Severens, B. Nienhuis, J. Duysens, P. Desain, N. Keijsers, and J. Farquhar, "Decoding sensorimotor rhythms during robotic-assisted treadmill walking for brain computer interface (BCI) applications," *PLoS ONE*, vol. 10, no. 12, p. e0137910 2015.

[52] N. Kwak, K. Müller, and S. Lee, "A lower limb exoskeleton control system based on steady state visual evoked potentials," *Journal of Neural Engineering*, vol. 12, no. 5, p. 056009 2015.

[53] A. R. C. Donati, S. Shokur, E. Morya, D. S. F. Campos, R. C. Moioli, C. M. Gitti, P. B. Augusto, S. Tripodi, C. G. Pires, G. A. Pereira, F. L. Brasil, S. Gallo, A. A. Lin, A. K. Takigami, M. A. Aratanha, S. Joshi, H. Bleuler, G. Cheng, A. Rudolph, and M. A. L. Nicolelis, "Long-Term Training with a Brain-Machine Interface-Based Gait Protocol Induces Partial Neurological Recovery in Paraplegic Patients," *Scientific Reports*, vol. 6, no. 1, p. 30383 2016.

[54] Y. Zhang, S. Prasad, A. Kilicarslan, and J. L. Contreras-Vidal, "Multiple kernel based region importance learning for neural classification of gait states from eeg signals," *Frontiers in Neuroscience*, vol. 11, no. April, pp. 1–11 2017.

[55] J. L. Contreras-Vidal, M. Bortole, F. Zhu, K. Nathan, A. Venkatakrishnan, G. E. Francisco, R. Soto, and J. L. Pons, "Neural decoding of robot-assisted gait during rehabilitation after stroke," *American Journal of Physical Medicine & Rehabilitation*, vol. 97, no. 8, pp. 541–550 2018.

[56] K. Lee, D. Liu, L. Perroud, R. Chavarriaga, and J. d. R. Millán, "A brain-controlled exoskeleton with cascaded event-related desynchronization classifiers," *Robotics and Autonomous Systems*, vol. 90, pp. 15–23 2017.

[57] W. Park, G. H. Kwon, Y.-H. Kim, J.-H. Lee, and L. Kim, "EEG response varies with lesion location in patients with chronic stroke," *Journal of NeuroEngineering and Rehabilitation*, vol. 13, no. 1, p. 21 2016.

[58] E. López-Larraz, F. Trincado-Alonso, V. Rajasekaran, S. Pérez-Nombela, A. J. Del-Ama, J. Aranda, J. Minguez, A. Gil-Agudo, and L. Montesano, "Control of an ambulatory exoskeleton with a brain-machine interface for spinal cord injury gait rehabilitation," *Frontiers in Neuroscience*, vol. 10, no. August, p. 359 2016.

[59] A. Kilicarslan, R. G. Grossman, and J. L. Contreras-Vidal, "A robust adaptive denoising framework for real-time artifact removal in scalp EEG measurements," *Journal of Neural Engineering*, vol. 13, no. 2, p. 026013 2016.

[60] Z. Li, J. E. O'Doherty, T. L. Hanson, M. Lebedev, C. S. Henriquez, and M. a. L. Nicolelis, "Unscented kalman filter for brain-machine interfaces," *PLoS ONE*, vol. 4, no. 7, p. e6243 2009.

[61] G. Welch and G. Bishop, "An introduction to the kalman filter," *University of North Carolina Website* 2006.

[62] R. Faragher, "Understanding the basis of the kalman filter via a simple and intuitive derivation," *IEEE Signal Processing Magazine*, vol. 29, no. 5, pp. 128–132 2012.

[63] S. Dangi, A. L. Orsborn, H. G. Moorman, and J. M. Carmena, "Design and analysis of closed-loop decoder adaptation algorithms for brain-machine interfaces," *Neural Computation*, vol. 25, no. 7, pp. 1693–1731 2013.

[64] T. C. Bulea, J. Kim, D. L. Damiano, C. J. Stanley, and H.-S. Park, "Prefrontal, posterior parietal and sensorimotor network activity underlying speed control during walking," *Frontiers in Human Neuroscience*, vol. 9, no. May, p. 247 2015.

[65] D. A. Winter, "Kinematic and kinetic patterns in human gait: Variability and compensating effects," *Human Movement Science*, vol. 3, no. 1-2, pp. 51–76 1984.

[66] T. P. Luu, Y. He, S. Brown, S. Nakagame, and J. L. Contreras-Vidal, "Gait adaptation to visual kinematic perturbations using a real-time closed-loop brain-computer interface to a virtual reality avatar," *Journal of Neural Engineering*, vol. 13, no. 3, p. 036006 2016.

[67] A. Presacco, R. Goodman, L. Forrester, and J. L. Contreras-Vidal, "Neural decoding of treadmill walking from noninvasive electroencephalographic signals," *Journal of Neurophysiology*, vol. 106, no. 4, pp. 1875–1887 2011.

[68] A. Presacco, L. W. Forrester, and J. L. Contreras-Vidal, "Decoding intra-limb and inter-limb kinematics during treadmill walking from scalp electroencephalographic (EEG) signals," *IEEE Transactions on Biomedical Engineering*, vol. 20, no. 2, pp. 212–9 2012.

[69] T. P. Luu, Y. He, S. Brown, S. Nakagome, and J. L. Contreras-Vidal, "A closed-loop brain computer interface to a virtual reality avatar: Gait adaptation to visual kinematic perturbations," *International Conference on Virtual Rehabilitation (ICVR)*, pp. 30–37 2015.

[70] T. P. Luu, Y. He, S. Nakagame, J. Gorges, K. Nathan, and J. L. Contreras-Vidal, "Unscented Kalman filter for neural decoding of human treadmill walking from non-invasive electroencephalography," *38th Annual International Conference of the IEEE Engineering in Medicine and Biology Society (EMBC)*, pp. 1548–1551 2016.

[71] D. Henz, A. John, C. Merz, and W. I. Schöllhorn, "Post-task effects on eeg brain activity differ for various differential learning and contextual interference protocols," *Frontiers in Human Neuroscience*, vol. 12, no. January, pp. 1–10 2018.

[72] M. Grosse-Wentrup, D. Mattia, and K. Oweiss, "Using brain-computer interfaces to induce neural plasticity and restore function," *Journal of Neural Engineering*, vol. 8, no. 2 2011.

[73] K. Lim, H. Lee, J. Yoo, H. Yun, and H. Hwang, "Efficacy of mirror therapy containing functional tasks in poststroke patients," *Annals of Rehabilitation Medicine*, vol. 40, no. 4, p. 629 2016.

[74] J. Wang, C. Fritzsch, J. Bernarding, S. Holtze, K. H. Mauritz, M. Brunetti, and C. Dohle, "A comparison of neural mechanisms in mirror therapy and movement observation therapy," *Journal of Rehabilitation Medicine*, vol. 45, no. 8, pp. 410–413 2013.

[75] H. Thieme, J. Mehrholz, M. Pohl, J. Behrens, and C. Dohle, "Mirror therapy for improving motor function after stroke," *Stroke*, vol. 44, pp. 2013–2015 2013.

[76] D. McEwen, A. Taillon-Hobson, M. Bilodeau, H. Sveistrup, and H. Finestone, "Virtual reality exercise improves mobility after stroke," *Stroke*, vol. 45, no. 6, pp. 1853–1855 2014.

[77] A. Darekar, B. J. McFadyen, A. Lamontagne, and J. Fung, "Efficacy of virtual reality-based intervention on balance and mobility disorders post-stroke: a scoping review," *Journal of NeuroEngineering and Rehabilitation*, vol. 12, no. 1, p. 46 2015.

[78] R. W. Teasell, M. Murie Fernandez, A. McIntyre, and S. Mehta, "Rethinking the continuum of stroke rehabilitation," *Archives of Physical Medicine and Rehabilitation*, vol. 95, no. 4, pp. 595–596 2014.

[79] K. E. Laver, S. George, S. Thomas, J. E. Deutsch, and M. Crotty, "Virtual reality for stroke rehabilitation," *Cochrane Database of Systematic Reviews* 2015.